Numerical investigation of on-demand fluidic winglet aerodynamic performance and turbulent characterization of a low aspect ratio wing

A. Mondal, S. Chatterjee, A. McDonald Tariang, L. Prince Raj* and K. Debnath

Department of Aerospace Engineering and Applied Mechanics, Indian Institute of Engineering Science & Technology, Shibpur, Howrah 711103, India

Abstract. Drag reduction is significant research in aircraft design due to its effect on the cost of operation and carbon footprint reduction. Aircraft currently use conventional solid winglets to reduce the induced drag, adding extra structural weight. Fluidic on-demand winglets can effectively reduce drag for low-speed flight regimes without adding any extra weight. These utilize the spanwise airflow from the wingtips using hydraulic actuators to create jets that negate tip vortices. This study develops a computational model to investigate fluidic on-demand winglets. The well-validated computational model is applied to investigate the effect of injection velocity and angle on the aerodynamic coefficients of a rectangular wing. Further, the turbulence parameters such as turbulent kinetic energy (TKE) and turbulent dissipation rate are studied in detail at various velocity injections and at an angle of 30°. The results show that the increase in injection velocity shifted the vortex core away from the wing tip and the increase in injection angle shifted the vortex core in the vertical direction. Further, it was found that a 30° injection is efficient among all injection velocities and highly efficient at a velocity ratio of 3. This technology can be adopted in any aircraft, effectively working at various angles of attack. The culmination of this study is that the implementation of fluidic winglets leads to a significant reduction in drag at low speeds for low aspect ratio wings.

Keywords: drag reduction method; fluidic winglet; induced drag; turbulent jets; wingtip injection

1. Introduction

One of the most sought-after research fields in the aviation industry is aircraft drag reduction, and numerous methods have been developed subsequently. Due to the lift generation, a vorticity field is formed at the wing tips as a by-product, and it trails downstream of the trailing edge. These wingtip vortices downstream of the wing induce a downwash in the neighborhood of the wing itself, resulting in the generation of induced drag. The induced drag remains a major concern for the aviation industry as they pose a potential hazard to flight safety, along with its depreciative effect on aerodynamic efficiency. In general, induced drag accounts for up to 40% of the aircraft drag during cruise (Kroo 2001). Over the past few decades, there has been a significant incentive to understand the structure and evolution of wingtip vortices in the near and far fields to design effective control strategies capable of reducing their undesirable effects (Deslich and Gunasekaran

---

*Corresponding author, Assistant Professor, E-mail: plraj@aero.iiests.ac.in

2019, Gursul and Wang 2018, Liu *et al*. 2021).

Numerous studies have been conducted to study the stability, structure, and propagation of the trailing vortices behind the wing (Crow 1970). The most rudimentary solution to obstruct the formation of trailing vortices was to mount passive ad-hoc devices on wing tips known as winglets. This protrusion of the wing from the tip aimed to increase the effective wing aspect ratio by physically hindering the creation of a wingtip vortex. Satisfactory results were achieved with this technology, with up to a 20% reduction of induced drag and roughly a 9% increase in wing efficiency (Whitcomb 1976). Different shapes and geometries of winglets were tested to arrive at an optimal shape for better efficiency (Lappas and Ikenaga 2019, Narayan and John 2016, Panagiotou *et al*. 2014). However, adding a new surface inevitably increased skin friction drag and structural weight. The winglets could not be optimized for different flight conditions as they were fixed by nature, while induced drag decreases with velocity. Nevertheless, these winglets have been extensively used by aircraft manufacturers. Recently, there has been increasing interest in employing active wingtip devices as they were found to provide an effective control authority over trailing vortices and could exploit the inherent instabilities present in them, therefore improving the aerodynamic characteristic of the corresponding lifting surface.

Various research teams around the world have developed a variety of active flow control techniques. For instance, Ayers and Wilde (1956) was the first study on spanwise blowing from wing-tips of a low aspect ratio wing as a flow control technique and its effect on the aerodynamic characteristics of the wing. They found that the wing loading increased towards the wing tips and the wing effective aspect ratio increased with spanwise blowing. With a certain momentum discharge, the maximum lift coefficient increased by 36%, whereas the lift slope increased by 19%. The drag coefficient was reduced by around 5% for a given lift coefficient and the stall angle increased by 18%. Mineck (1995) experimentally and analytically assessed the effect of spanwise blowing at the tip of a moderate aspect-ratio swept wing and their potential aerodynamic benefits. Results indicated that blowing with jets for wings with longer chords increased the lift near the tip and reduced drag for low Mach numbers, whereas jets for short-chord wings were ineffective. Elie Carafoli (1962) formulated a theory based on Prandtl's lifting theory and conducted experiments on lateral blowing from wing tips of a straight wing of aspect ratio 2. It was observed that the lift increased with jet injection due to the effective enlargement of the wingspan brought about by the jet. Later, Carafoli and Camarasescu (1971) extended the study for small-aspect-ratio wings and observed that variations in the lift are more intense for smaller aspect ratio wings.

Further experimental work was conducted on lateral blowing, and a favorable effect on drag for specific conditions was observed (White 1963). An experimental investigation on the effect of discrete wingtip jets from a rectangular wing was investigated, and aerodynamic improvements were found even at small jet injections (Wu *et al*. 1983). Tavella *et al*. (1985, 1988) conducted more studies on spanwise jet injection with the variation of jet intensities, aspect ratio, and angle of attack of the wing. Later he attempted lateral and roll control of the aircraft with spanwise jet blowing (Tavella *et al*. 1986). Further, Briggs and Schwind (1983) investigated the concept of lateral blowing devices from the wingtips of STOL aircraft to enhance lift characteristics. Experimental works by Coimbra and Catalano (2002) investigated the effect on the vortex drag of a rectangular low-aspect wing at low speed using a novel tip-blowing system consisting of three Coanda-type jets. An increase in lift and pitching moment was observed, with a decrease in drag for most of the configurations tested. Further, Gunasekaran and Gerham (2018) investigated the effect of chordwise slots on aerodynamic efficiency and wingtip vortex on a NACA0012 wing experimentally. The results show that the implementation of the slots reduced the drag coefficients

by upto 20% of the base variant wing.

Duraisamy and Baeder (2003) validated the mean flow field using a high-order accurate scheme with appropriately refined meshes. Childs (1986) also performed a computational study investigating lift augmentation due to spanwise blowing. Wood and Roberts (1988) investigated the feasibility of vortex control over the delta wing with tangential mass injections at the leading edge. While most studies employed wingtip blowing Okada and Hiraoka (2003) investigated the lift augmentations achieved using wingtip suction. Lim (1994) conducted a numerical study comparing the effects of axial wingtip blowing with spanwise wingtip blowing. Skarolek and Karabelas (2016) numerically simulated the effect of blowing near the trailing edge using large slot areas and low-velocity jets to find an energy-efficient solution to wingtip blowing. Vedamanickam *et al.* (2018) studied the aerodynamics of a two-bladed propeller model with a passive tip jet to reduce the tip vortex strength. It is observed that the slots in the propeller blade cause a substantial change in skin friction of the blade surface, consequently affecting the performance of the propeller.

Simpson *et al.* (2002) took up a study to reduce wake turbulence by using spanwise jet blowing for faster dissipation of wingtip vortices. They noted that the vortices dissipate faster when wingtip blowing is applied. Margaris and Gursul (2004, 2010) experimented with spanwise blowing with different slots and found that the vortex location, strength, and nature change with different slots and injection intensities. Holloway and Richardson (2007) took up another study to investigate the vortex core distortion from the development of vortex size and speed of trailing vortex of an aspect ratio of 5 wing with spanwise tip jets. Experiments were conducted for a wide range of tip jet blowing intensities for a fixed-wing incidence. It was found that the turbulence values increased tenfold with the activation of wingtip blowing compared to the case of the natural vortex. The vortex core rapidly grew, and mean velocity gradients reduced simultaneously with this rapid decay of the turbulence levels downstream. The effects of the higher rate of blowing were similar yet more pronounced.

In a recent study, Dghim *et al.* (2014, 2016) used high aspect ratio synthetic jets at the wing tip with a curved slot for jet injection to study the turbulence parameters. They noted that with the evolution of the vortex, the turbulent kinetic energy in the shear layer seemed to be drawn into the vortex core and then spread outward. The turbulence levels measured within the vortex core and the shear layer intensified with the operation of synthetic jets. This resulted in vortex attenuation by enhanced mixing and accelerated diffusion as it developed downstream. Flow visualization results showed turbulent diffusion in the vortex core to be more pronounced with higher momentum coefficients. A nearly 30% decrease in the core axial vorticity was reported with the use of synthetic jets. Dutta *et al.* (2022) numerically investigated the effect of spanwise blowing using a fluidic winglet on a low aspect ratio wing. They simulated the effects of various velocities spanwise jet injections on the aerodynamic characteristics and inspected the variations in turbulence parameters. Their work mainly focused on using low-velocity jets to obtain significant drag reduction and find optimal jet velocity for efficient vortex attenuation and drag reduction in small UAVs.

The current work herein explores further the effects of steady spanwise blowing with high injection velocities at different injection angles from wing tips, unlike the other studies with normal injection. A numerical study was undertaken to simulate a wing of aspect ratio 3 and airfoil K3311 in freestream, with constant spanwise injection out of the wing tips. Low subsonic freestream conditions were used, coinciding with the operating condition of most micro UAVs. A parametric study with varying injection jet velocities and injection jet angles was conducted to find
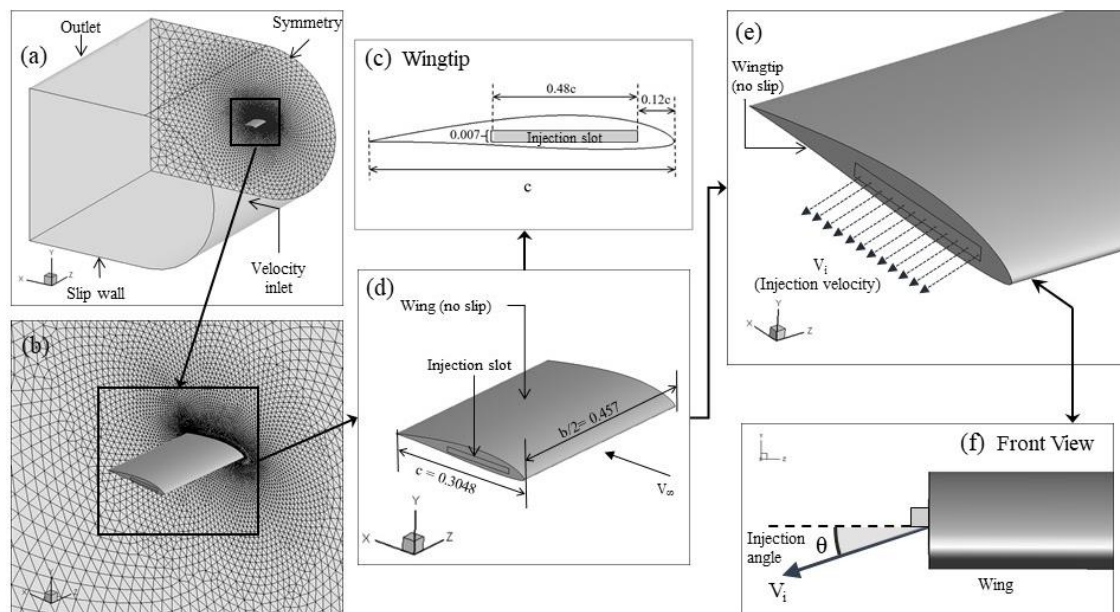
Fig. 1 Meshing and boundary conditions

optimal conditions for using fluidic winglets in low-speed subsonic flights, which the other studies were unsuccessful in concluding. Effects of various injection velocities ranging from low velocities up to multiple times of freestream velocity were investigated. Performance parameters such as lift coefficient, drag coefficient, and lift-to-drag ratio were monitored to study its variation with the injection jets. A lack of research on turbulence parameters with spanwise injection motivated close examination of turbulence and vorticity parameters for the different cases to understand the characteristics of the evolution of the modified vortex system and its interactions with the wing. Further, the correlation between turbulence characteristics and aerodynamic coefficients was closely studied to give more insight into flow physics.

2. Methodology and computational modelling

A low Reynolds number airfoil, K3311, which is commonly used in small UAVs and MAVs, is considered for simulation. After exploring the aerodynamic characteristics of many airfoils, K3311 was selected because of the better lift coefficient at high angles of attack, even at a very low Reynolds number of 60,000, and smooth stall characteristics compared to similar other airfoils. The airfoil coordinates are obtained from and the chord length of 0.3048 m (12 in.) was taken from literature (Selig *et al*. 1995). This airfoil generates a 3D model of the rectangular, unswept, untwisted wing with an aspect ratio AR=3 and a semi-span of 0.4572 m. A rectangular injection slot parallel to the chord is cut at the wingtips through which the spanwise flow is injected. It is placed between the front and rear spars of the wing box, generally positioned at 12% and 60% of the tip chord with a height of 7mm, ensuring enough clearance from the top and bottom surfaces. Fig. 1 shows the computational domain, injection slot position, mesh, and boundary condition used for the present study.

Numerical simulation of the flow field has been carried out using a Finite Volume based steady Reynolds averaged three-dimensional Navier Stokes equations solver. The SIMPLEC (Semi-Implicit Method for Pressure-Linked Equations-Consistent) algorithm (Van Doormaal and Raithby 1984) is used for pressure velocity coupling. The SST (Shear Stress Transport) *k-ω* turbulence model (Menter 1993, 1994) is used because it can accurately capture the near field viscous sub-layer and switch to *k-ε* behavior in the far field, which is relatively less resource intensive. This model is known mainly for its good behavior during adverse pressure gradients and flow separation. However, it produces large turbulence levels in regions experiencing large normal strain like stagnation regions and strong acceleration. This tendency is quite less pronounced than in the *k-ω* model, though in the SST *k-ω* model, $k = $ TKE and $\omega = \varepsilon/k$ are the specific dissipation rate and $\varepsilon = $ pseudo dissipation rate. The complete set of governing equations are

$$\frac{\partial \bar{u}_i}{\partial x_i} = 0 \tag{1}$$

$$\rho.\bar{u}_j \frac{\partial \bar{u}_i}{\partial x_j} = \frac{\partial}{\partial \bar{x}_j}\left[-\bar{p}.\delta_{ij} + \mu\left(\frac{\partial \bar{u}_i}{\partial \bar{x}_j} + \frac{\partial \bar{u}_j}{\partial \bar{x}_i}\right) - \rho\bar{u}_i' u_j'\right] \tag{2}$$

$$\frac{\partial(\rho k)}{\partial t} + \frac{\partial(\rho k u_i)}{\partial x_i} = \frac{\partial}{\partial x_j}\left[\Gamma_k \frac{\partial k}{\partial x_j} + G_k - Y_k + S_k\right] \tag{3}$$

$$\frac{\partial(\rho\omega)}{\partial t} + \frac{\partial(\rho\omega u_j)}{\partial x_j} = \frac{\partial}{\partial x_j}\left[\Gamma\omega \frac{\partial \omega}{\partial x_j}\right] + G_\omega - Y_\omega + D_\omega + S_\omega \tag{4}$$

Here ρ represents the density of free stream air, $\bar{u}_i, \bar{u}_j$ are time-averaged velocities in mutually perpendicular directions and $\bar{p}$ represents the time-averaged pressure force. G_k and G_ω represent the generation of TKE and ω, respectively. Γ_k and Γ_ω represent the effective diffusivity of TKE and ω, respectively. Y_k and Y_ω represent the dissipation of TKE and ω, respectively. D_ω represents the cross-diffusion term. S_k and S_ω represent secondary source terms. Since the freestream Mach number is 0.06, the flow domain is assumed to be incompressible, i.e., free stream density is constant.

3. Grid Independence study and validation

Grid independence study is conducted with six computational meshes for a straight wing of AR=3, as shown in Table 1. Lift coefficient C_L is recorded for two different angles of attack $\alpha = -0.47^0$, 5.24^0 and $Re_c = 305,100$ for each mesh. It is evident from Table 1 that there is no significant change in C_L by refining the grid from case mesh M5 to M6. Thus grid independence is reached, and mesh M5 is chosen to prevent greater computational cost.

For validation, two-dimensional experimental data (Selig *et al.* 1995) obtained from the wind tunnel experiment is taken and converted to three-dimensional data using Prandtl's Lifting Line theory. The computational model is validated with a Reynolds number based on the mean aerodynamic chord $Re_c = 305100$, and a velocity of 19.245 m/s. The experimental and computational results are shown in Fig. 2, which shows that the numerical analysis results are in close agreement with the converted experimental data, with a minor deviation in the high angle of attack for the lift curve and a slight deviation in the drag coefficient. This may be because potential

Table 1 Number of elements used corresponding to mesh number and mesh independence study

Mesh Number	Elements (in millions)	C_L at 5.24°	C_L at -0.47°
M1	0.10	0.6322	0.2996
M2	0.18	0.6775	0.2910
M3	0.28	0.6865	0.3106
M4	0.38	0.6953	0.3123
M5	0.46	0.6956	0.3131
M6	0.55	0.6956	0.3132
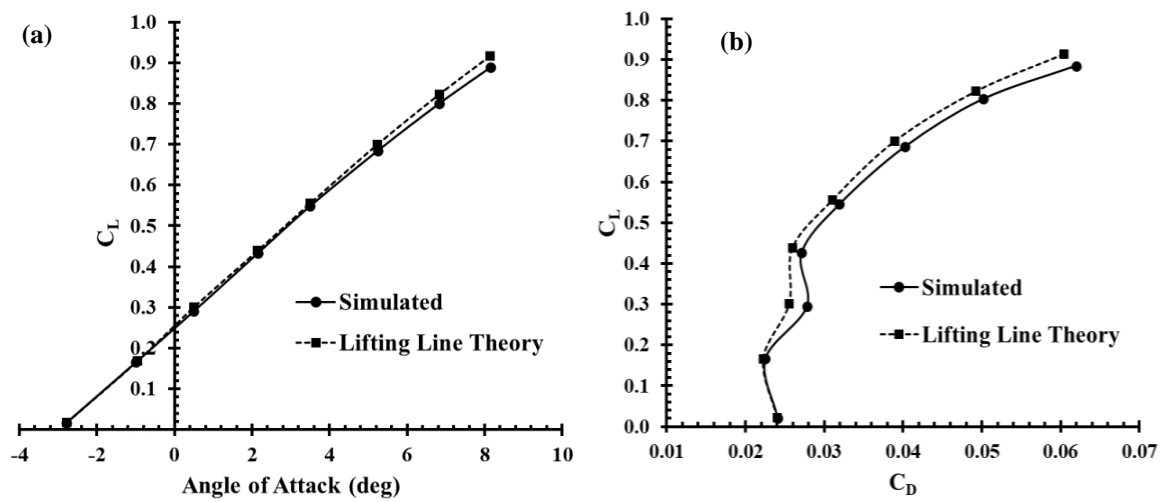
Fig. 2 Validation of computational model with lifting line theory

Table 2 Test cases used for investigation

CASES	Jet Injection Angle			
	$\theta=0°$	$\theta=30°$	$\theta=50°$	$\theta=70°$
	$V_i/V_\infty=0.5$	$V_i/V_\infty=0.5$	$V_i/V_\infty=0.5$	$V_i/V_\infty=0.5$
	$V_i/V_\infty=1.0$	$V_i/V_\infty=1.0$	$V_i/V_\infty=1.0$	$V_i/V_\infty=1.0$
	$V_i/V_\infty=1.5$	$V_i/V_\infty=1.5$	$V_i/V_\infty=1.5$	$V_i/V_\infty=1.5$
	$V_i/V_\infty=2.0$	$V_i/V_\infty=2.0$	$V_i/V_\infty=2.0$	$V_i/V_\infty=2.0$
Jet Injection	$V_i/V_\infty=2.5$	$V_i/V_\infty=2.5$	$V_i/V_\infty=2.5$	$V_i/V_\infty=2.5$
Velocity	$V_i/V_\infty=3.0$	$V_i/V_\infty=3.0$	$V_i/V_\infty=3.0$	$V_i/V_\infty=3.0$
	$V_i/V_\infty=3.5$	$V_i/V_\infty=3.5$	$V_i/V_\infty=3.5$	$V_i/V_\infty=3.5$
	$V_i/V_\infty=4.0$	$V_i/V_\infty=4.0$	$V_i/V_\infty=4.0$	$V_i/V_\infty=4.0$
	$V_i/V_\infty=4.5$	$V_i/V_\infty=4.5$	$V_i/V_\infty=4.5$	$V_i/V_\infty=4.5$
	$V_i/V_\infty=5.0$	$V_i/V_\infty=5.0$	$V_i/V_\infty=5.0$	$V_i/V_\infty=5.0$

flow theory does not account for nonlinearity. This concludes that the overall computational results are sufficiently accurate for this analysis within the aircraft's operating range.
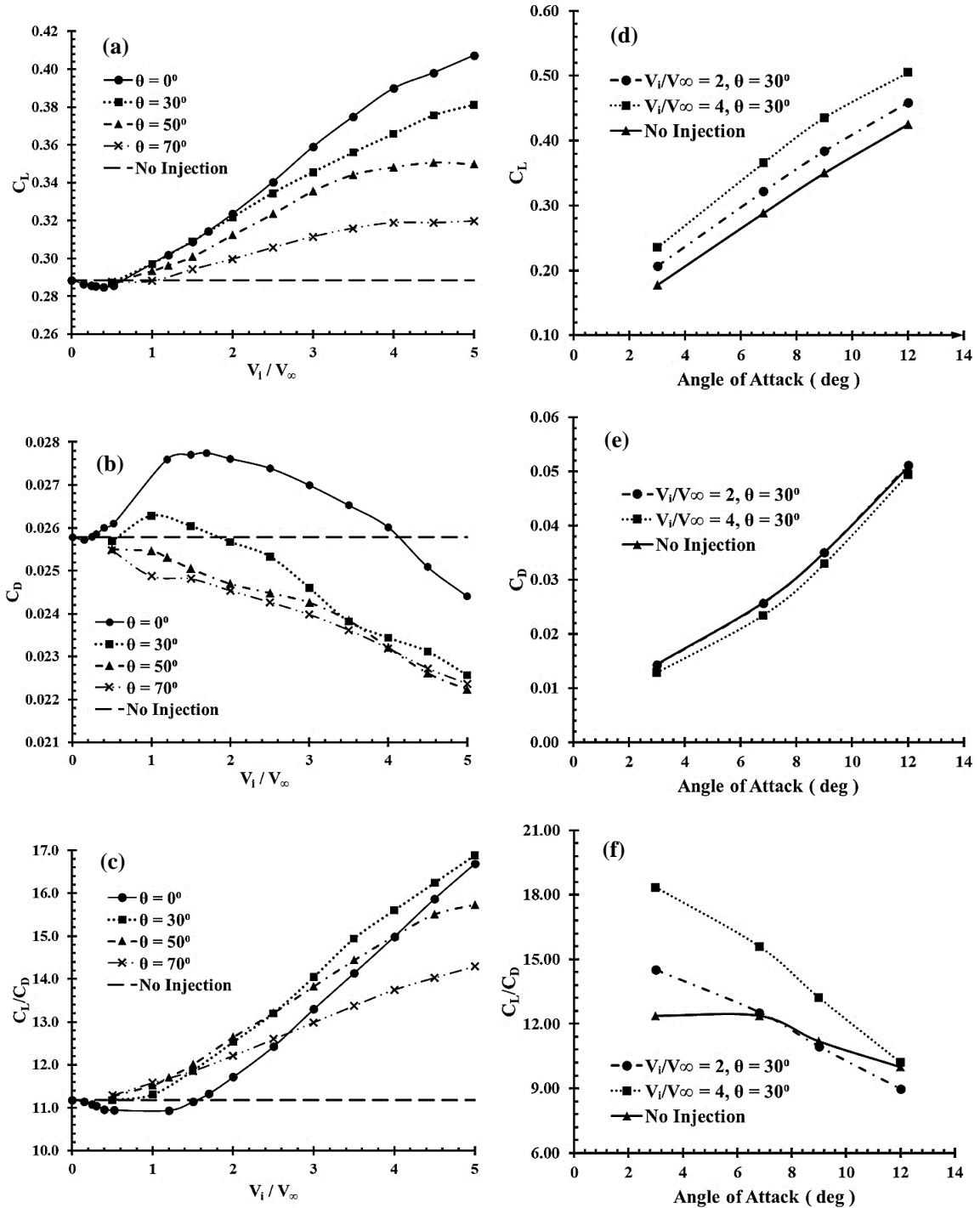
Fig. 3 (a) Lift Coefficient, (b) Drag Coefficient, and (c) Lift to Drag Ratio as a function of Injection Velocity Ratio with Different Injection Angle; (d) Lift Coefficient, (e) Drag Coefficient, and (f) Lift to Drag Ratio as a function of Angle of Attack with D

4. Results and discussion

4.1 Aerodynamic characteristics

Computational tests were conducted for the different cases, as shown in Table 2, and the results are discussed elaborately.

Overall aerodynamic characteristics were studied by investigating lift coefficient (C_L), drag coefficient (C_D), and lift to drag ratio (C_L/C_D) variations with injection velocity ratio (V_i/V_∞) and injection angle (θ) at an angle of attack of 6.81°. Fig. 3(a) shows the variation of C_L with injection velocity for different injection angles, which illustrates that the lift increases with the increase in injection velocity up to a range, and beyond that range, no significant increase in lift is observed. It is worth mentioning that the C_L gradient changes at the given injection angle, which shows that the injection angle also affects the lift generation significantly same as reported by the literatures (Ayers and Wilde 1956, Ej Carafoli and Camarasescu 1971). Further, it is noted that with the increase in injection angle, the lift decreases but is always greater than in the no-injection case. Fig. 3(b) shows the drag coefficient (C_D) for various injection angles and velocities, showing that the drag behaves differently from the lift coefficient. For the normal direction injection case ($\theta=0°$), the drag increases rapidly with the increase in injection velocity ratio up to some extent. Beyond that, the drag gradually reduces and reaches a minimum for the maximum injection ratio. Further, for injection angle 30°, the drag slightly increases up to a specific limit and decreases with a further increase in jet injection velocity. However, for injection angles 50° and 70°, the drag coefficient decreases gradually with the increase in the injection ratio.

To determine the injection velocity and angle for best aerodynamic performance, aerodynamic efficiency is analyzed by scrutinizing the variation of C_L/C_D as plotted in Fig. 3(c). The C_L/C_D for injection angle 0° reduced at the lower injection velocity ratios and gradually increased after the velocity ratio of 1.5, possibly due to the drag coefficient increase. Overall, it is found that the best performance corresponds to the injection angle of 30° and the velocity ratio of 5 (at high injection velocity). To get more insight into the aerodynamic performance, different angle of attack simulations were conducted at an injection angle of 30°. Fig. 3(d) to 3(f) show the variation of aerodynamic coefficients as a function of angle of attack with different injection velocity ratios for injection angle 30° along with the no-injection case. It is found that the lift and drag coefficients of cases with injection follow the same trend as in the no-injection case, as shown in Fig. 3(d) and 3(e). Further, the lift coefficient at injection angle 30° is higher for all angles of attack while the drag is also minimum. Hence, the C_L/C_D is also high for the 30° injection at all angles of attack. Further, it is found that the C_L/C_D decreases with the increase of the angle of attack.

To gain better insight into flow physics, the streamlines are plotted in Fig. 4(a)-4(h). Although many simulations are conducted, only three injection velocity ratios, $V_i/V_\infty=1$, 3, and 5, and injection angles $\theta=0°$ and 30° are used for further investigations. However, the no-injection case is also added in the further investigation for better comparison. More streamlines were specifically added near the wingtip to investigate the flow changes and effects of spanwise injection in detail. Fig. 4(a) shows the wing orientation considered in the present analysis, and Fig. 4(b) shows the normal wingtip formation without any jet injection. It is observed that the flow curls around the wingtip, and the vortex continues downstream at no injection. Fig. 4(c) illustrates the streamlines around the wing tip at an injection ratio of 1 and 0 degrees, showing a slight increase in primary vortex size. It is observed that the vortex is slightly pushed away from the wing tip at the injection ratio of 1 and injection angle of 30°, as shown in Fig. 4(d). Further increase in velocity ratio to 3 at
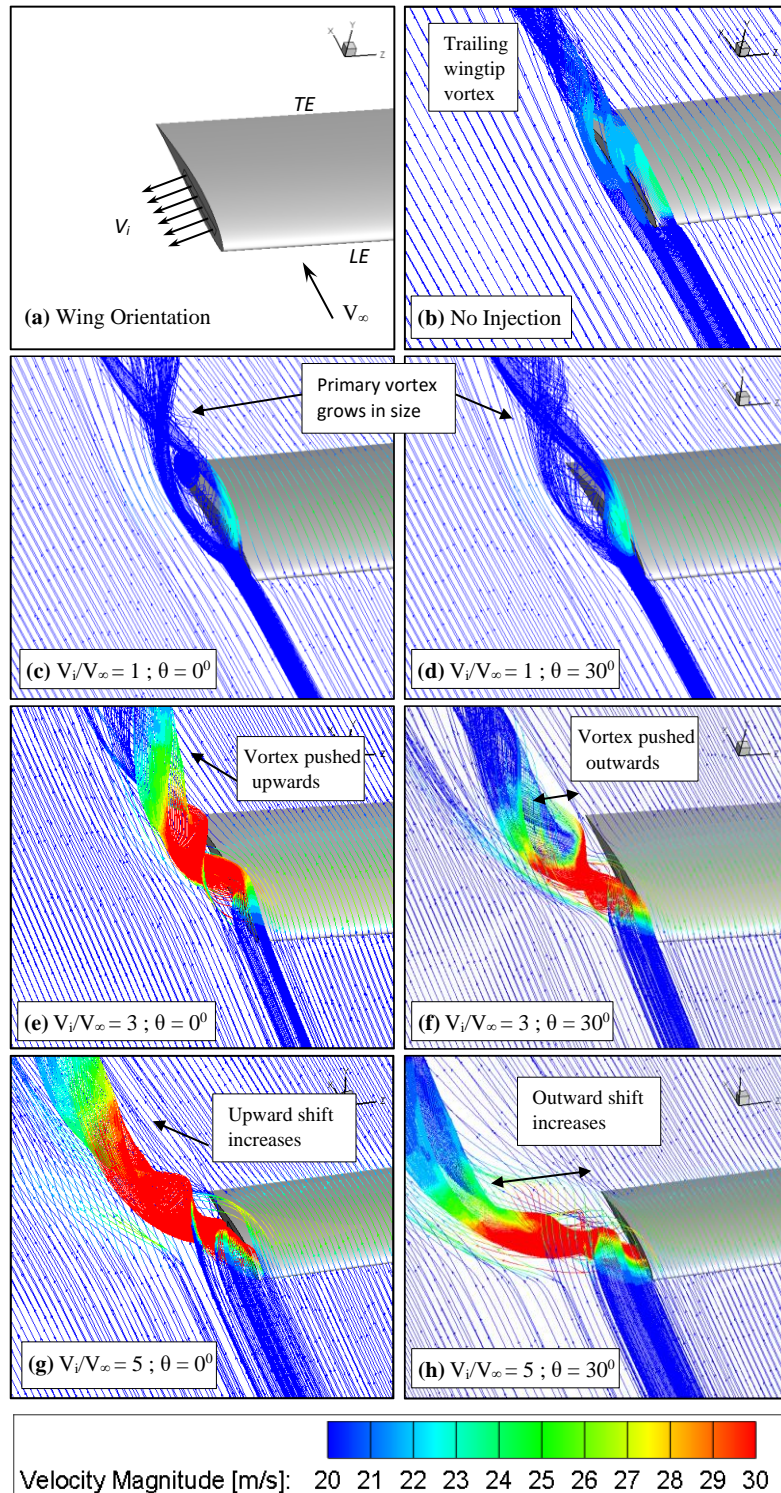
Fig. 4 (a) Wing Orientation, 3D Streamline Plots for (b) No Injection, (c) V_i/V_∞=1; θ=0°, (d) V_i/V_∞=1; θ=30°, (e) V_i/V_∞=3; θ=0°, (f) V_i/V_∞=3; θ=30°, (g) V_i/V_∞=5; θ=0°, (h) V_i/V_∞=5; θ=30°
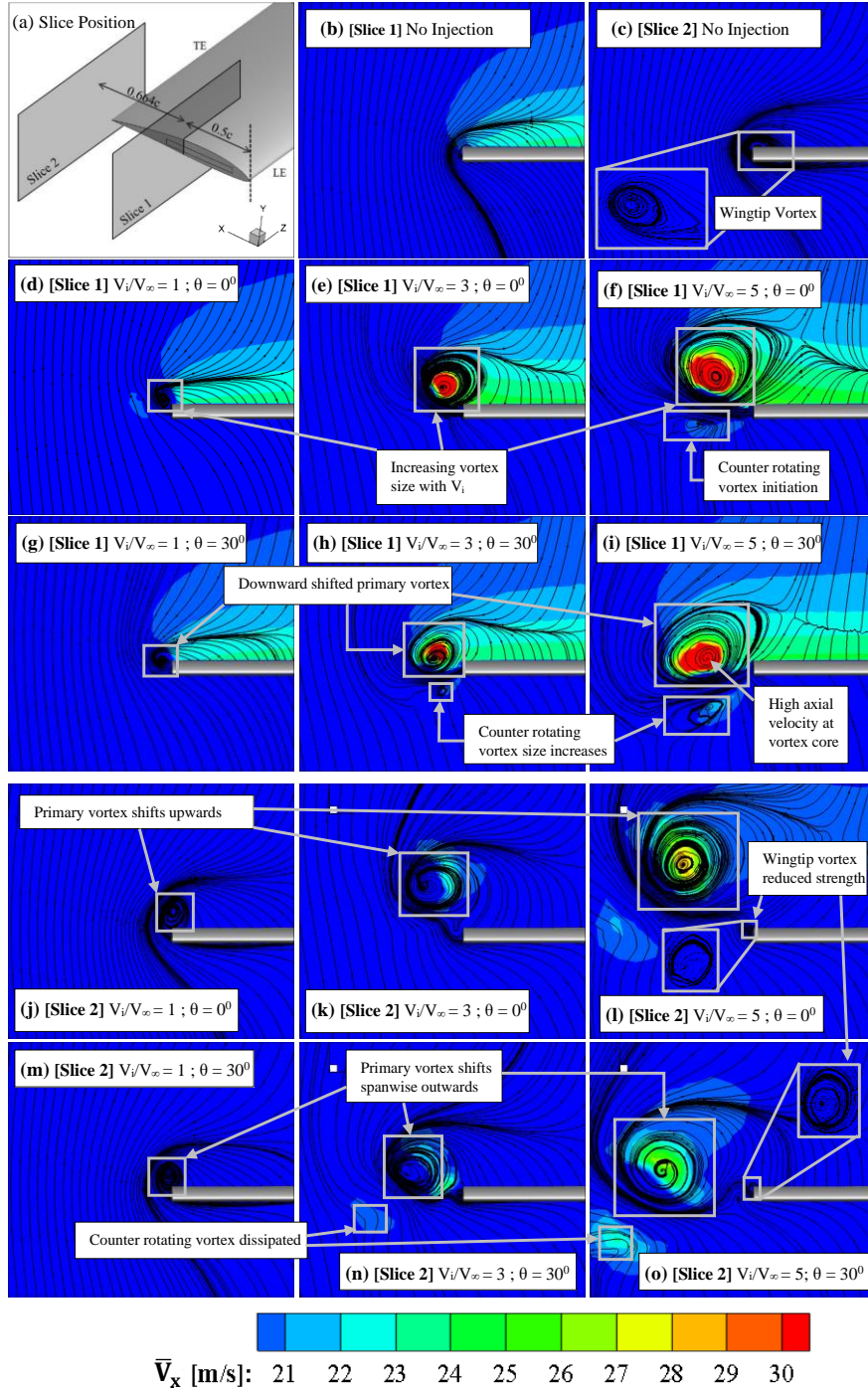
Fig. 5 (a) Slice Location, 2D Streamline Plots for- (b) [Slice 1] No Injection, (c) [Slice 2] No Injection, (d) [Slice 1] V_i/V_∞=1; θ=0°, (e) [Slice 1] V_i/V_∞=3; θ=0°, (f) [Slice 1] V_i/V_∞=5; θ=0°, (g) [Slice 1] V_i/V_∞=1; θ=30°, (h) [Slice 1] V_i/V_∞=3; θ=30°, (i) [Slice 1] V_i/V_∞=5; θ=30°, (j) [Slice 2] V_i/V_∞=1; θ=0°, (k) [Slice 2] V_i/V_∞=3; θ=0°, (l) [Slice 2] V_i/V_∞=5; θ=0°, (m) [Slice 2] V_i/V_∞=1; θ=30°, (n) [Slice 2] V_i/V_∞=3; θ=30°, (o) [Slice 2] V_i/V_∞=5; θ=30°

an injection angle of 0° increases the size of the vortex, and the vortex slightly shifts upwards, as shown in Fig. 4(e).

Further, at injection angle 30°, the vortex shifts outward, as shown in Fig. 4(f). The vortex shifting phenomena is intensified with a further increase in injection velocity ($V_i/V_∞=5$), which is evident from Figs. 4(g) and 4(h). The vortex shift in the present study agrees with the results found in the computational investigations in the literature (Lim 1994). In Fig. 4(h), it is observed that the outward-shifted vortex modified the flow field such that the flow goes above and below the outward-pushed vortex as if it was a part of the wing. Thus, this vortex-shifting phenomenon increases the effective wingspan and aspect ratio, which results in the apparent increase in lift and reduction in drag.

To further investigate the vortex shifting phenomena, an analysis was conducted on the 2D streamlines of the slices over the wing along the spanwise direction (i.e., normal to wing chord). The 2D streamlines are visualized on two plane slices, one at the mid-chord of the wing (slice 1) and the other slice placed behind the trailing edge of the wing (slice 2), as shown in Fig. 5(a). The wingtip vortex generation and evolution for the simulation without injection are clearly seen in Fig. 5(b) and 5(c). Further, in Fig. 5(d)-5(i), the effect of injection angle and velocity ratio on the flow phenomena at mid-chord (slice 1) is illustrated. It is observed from Fig. 5(d)-5(f) that the increase in injection velocity increases the vortex growth, and in particular, a counter-rotating vortex begins to form at the velocity ratio 5.

Similarly, Fig. 5(g) to 5(i) shows the effect of injection angle ($θ=30°$) on the flow behaviour. It is observed that the increase in injection velocity increases the vortex growth and shifts downwards. Further, the counter-rotating vortex formation phenomena are more substantial for 30^0 injections, with an eminent counter vortex formed for velocity ratio 5. Similar counter-rotating vortices were found in the parametric studies (Margaris and Gursul 2010) and wind tunnel experiments (Wu *et al*. 1983) in the literature. It is worth mentioning that in the central region of the primary vortices, the axial flow velocity is high, and the flow accelerates inside the vortex core.

Fig. 5(j)-5(o) show the streamlines at slice 2, which is placed behind the wing's trailing edge, where the wingtip vortex is generally fully developed. In Fig. 5(j) to 5(l), the effects of injection velocity on the primary vortex are seen for an injection velocity of 0°. It is easily noticeable that the size of the vortices increases and shifts upward when compared to slice 1 (Fig. 5(d) to 5(f)). Moreover, the vortex size on the wing tips is minimal, which may be the reason behind the drag reduction. Fig. 5(m)-5(o) illustrates the streamlines at slice 2 for injection angle 30° at various injection ratios. It is found that the vortices are shifted outward at 30° injection angle, which is quite the opposite of the phenomenon for the zero injection angle results. The dissipated counter-rotating vortices region can also be easily observed in Fig. 5(n) and 5(o). As these primary vortices are farther away from the wing, the wing experiences an apparent increase in aspect ratio and, thus, a reduction in induced drag. These results concur with the numerical studies in the literature (Childs 1986), where similar vortex displacement and lift augmentations were noted.

Pressure distribution is studied by monitoring pressure variation at eight equidistant chordwise slices over the wing, as shown in Fig. 6(a). The main objective is to investigate the pressure variation in different jet injection cases to get insight into the C_L and C_D variations. The pressure distribution for no injection is illustrated in Fig. 6(b). In Fig. 6(c) and 6(d), the pressure distribution on the wing sections (slices) for the wingtip jet injection ratio of 1 at 0° and 30° injection angles are presented. It is observed that the pressure change is dramatic and is more prominent for the 0° injection angle than the 30°. Further increase in the injection velocity ratio to
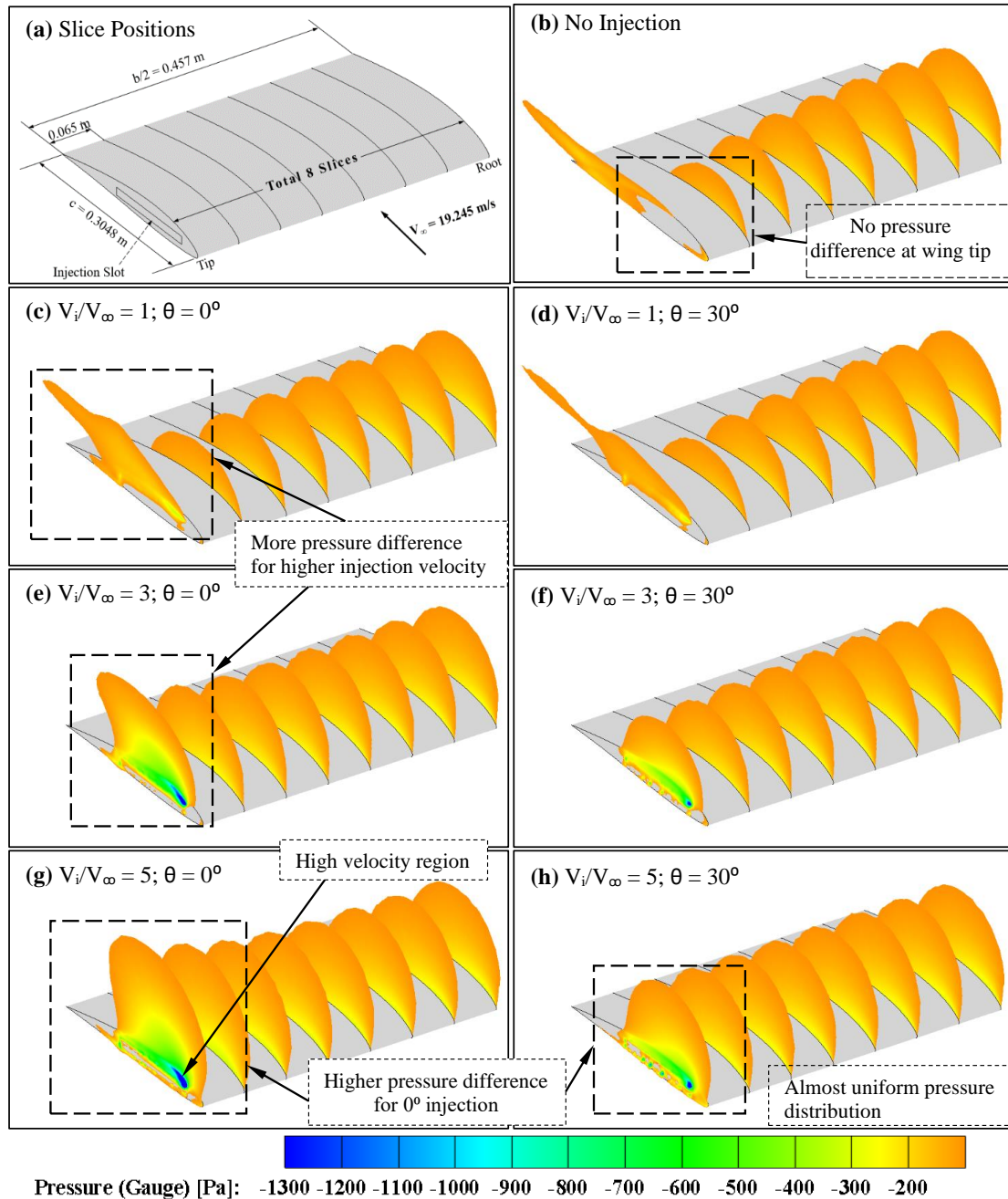
Fig. 6 (a) Positions of Slices over Wing, Contour Plots of Pressure around Wing (b) for No Injection, at V_i/V_∞=1 (c) θ=0°, (d) θ=30°, at V_i/V_∞=3 (e) θ=0°, (f) θ=30° and at V_i/V_∞=5 (g) θ=0°, (h) θ=30°

3 decreases the pressure as shown in Fig. 6(e) and 6(f). An increase in pressure difference is observed, which may be the primary cause of lift increase with increased jet injection velocity (Ayers and Wilde 1956). Also, it is observed that the pressure difference is high for injection angle
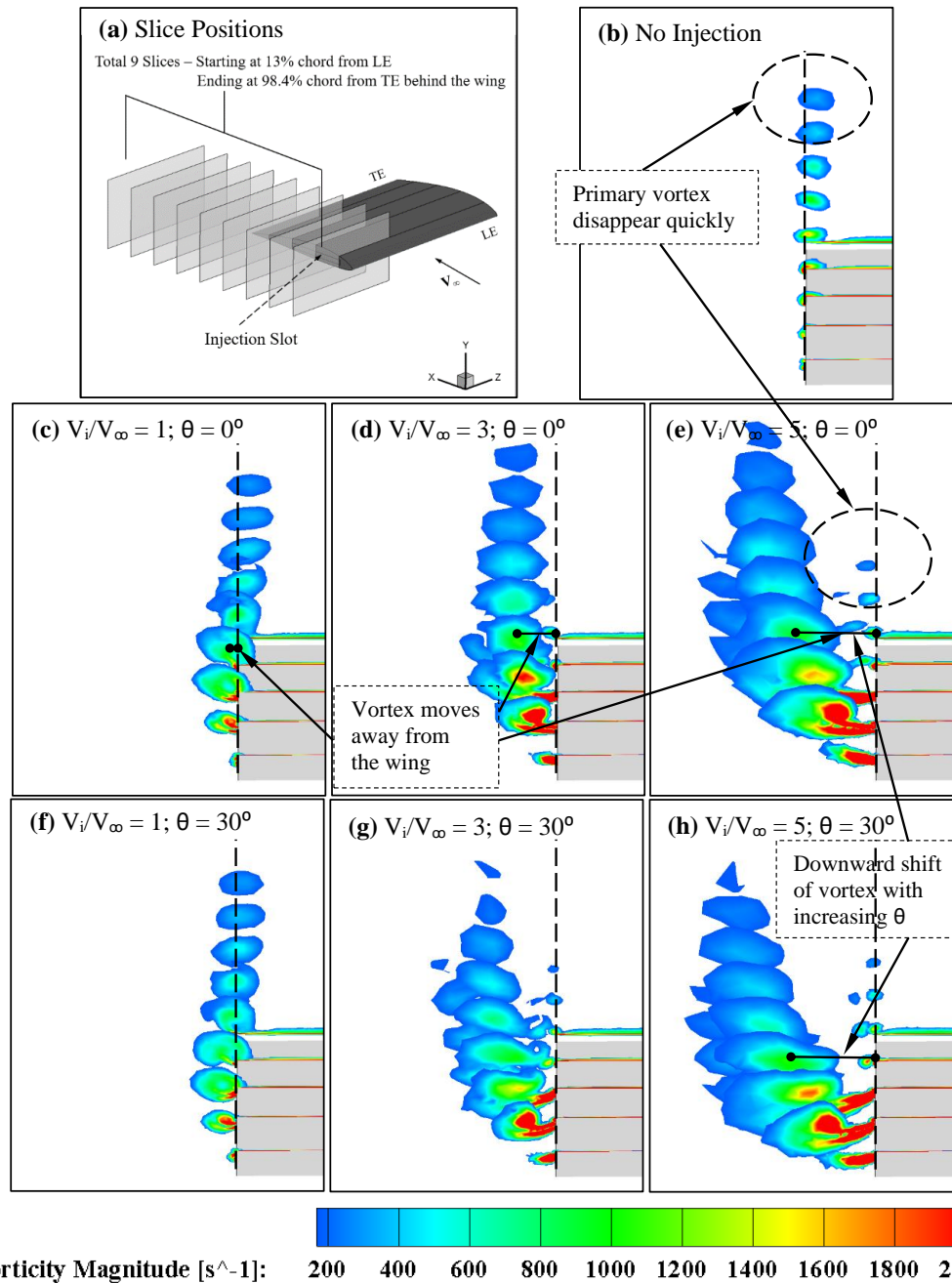
Fig. 7 (a) Positions of Slices, Contour Plots of Vorticity Magnitude around Wing (b) for No Injection, at θ=0° (c) V_i/V_∞=1, (d) V_i/V_∞=3, (e) V_i/V_∞=5 and at θ=30° (f) V_i/V_∞=1, (g) V_i/V_∞=3, (h) V_i/V_∞=5

0° compared to 30°. Similar effects are observed at velocity injection ratio 5, as shown in Fig. 6(g) and 6(h). Overall, the pressure difference is higher for 0° injection than 30°, resulting in high lift coeffecinent in the 0° case, which is already seen in the C_L curve plots illustrated in Fig. 3(a). Thus

it can be inferred that a reduction in lift that occurs with the increase in injection angle is due to the low-pressure difference at the wingtip with angled jet injections.

Fig. 7(a)-7(h) shows the slices along the wing chord, starting at 13% chord position and ending at 98.4% chord position, and the vorticity variations at different injection angles and velocity ratios. Fig. 7(a) shows the location of 9 slices along the wing chord, and Fig. 7(b) shows the vorticity magnitude around the wing tip under no injection condition. Fig. 7(c)-7(e) illustrate the vorticity magnitude around the wing tip at an injection angle of zero degrees and various injection velocity ratios. It is found that the air injection slightly pushed the vorticity away from the wing at the velocity ratio of 1, as shown in Fig. 7(c). Further increase in velocity ratio ($V_i/V_\infty=3$) increased the movement of vorticity away from the wing tip, which is clearly seen in Fig. 7(d). It is observed that at a high injection velocity ratio ($V_i/V_\infty=5$), vorticity is pushed away from the wing surface, as shown in Fig. 7(e). Therefore, the cross-velocity gradient is reduced, reducing the turbulence production and streamlining the flow.

Moreover, separation is reduced, increasing the lift and reducing the drag. It is worth mentioning that a small part of the vortex remained attached to the wing surface at a low injection velocity ratio and produced a smaller area of influence over the wing than the without injection case. Further, Fig. 7(f) to 7(h) shows that the vortex shifted outward owing to the injection angle of 30°. However, some portion of vortices remains attached to the wing surface at a velocity ratio of 1 while vortices move further from the wing at higher injection velocities. Further, Fig. 7(c)-7(h) shows that for the same injection velocity ratio, the vortices move downward for the higher injection angle. Overall, the vortices detached from the wing; hence the airflow from the lower surface to the upper surface does not take place, and the pressure difference does not decrease, as observed in Fig. 6(b)-6(h). Hence, a higher lift is achieved while the fluidic winglet is activated.

4.2 Turbulent characteristics of the fluid winglet

The use of SST (Shear Stress Transport) k-ω turbulence model Turbulence parameter allows for the evaluation of Turbulent Kinetic Energy (TKE) and Specific Dissipation Rate (ω) and thus these were evaluated across the chordwise distance from the leading edge to the trailing edge. The eddy viscosity hypothesis is the basis of two-equation turbulence closure models like k-ω SST, which give information on TKE and ω as the output turbulence parameters. The TKE measures the scale of turbulent fluctuations, and the large TKE regions extract energy from the mean flow with larger fluctuating scales compared to the low TKE regions. The energy in the fluctuating motion, drawn from the mean flow field, is finally transformed into internal energy by the eddy cascading process. Therefore this energy is mainly dissipated and can not be used to produce the lift. Fig. 9(a)-9(h) shows the slice location, and the contours of TKE are shown for different injection velocity ratios with the angle of injection.

Fig. 8(a) and 8(b) show the slice locations and the TKE distribution without injection, respectively. It is seen that without spanwise injection, the large TKE regions are associated with the thin boundary layer on the wing. Fig. 8(c) shows that at the injection velocity ratio 1, the large TKE regions shifted to the outside of the wing, leaving lower TKE close to the wingtip. With the same injection velocity ratio, for the higher injection angles ($\theta=30°$), the downward shift of higher TKE regions can be observed in Fig. 8(d). Moreover, the regions with high TKE are larger at the trailing edge than the mid-wing regions.

Further, the regions with high TKE become large for a higher injection velocity ratio, as shown in Fig. 8(e). With increasing injection angle, a slight increase in the high TKE region is observed,
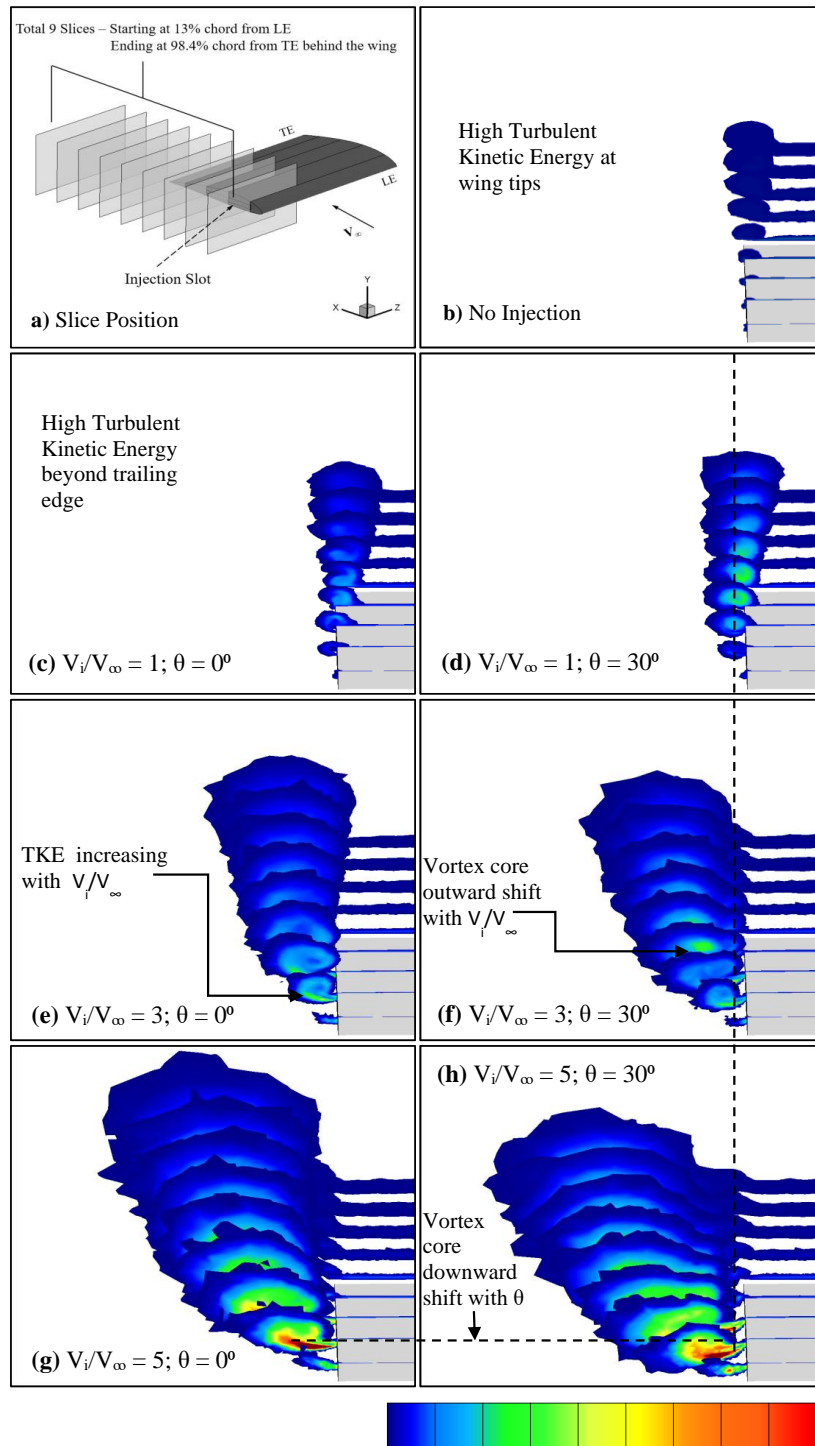
Fig. 8 (a) Slice Position; Contour plots for Turbulent Kinetic Energy (b) No Injection; (c) V_i/V_∞=1; θ=0°; (d) V_i/V_∞=1; θ=30°; (e) V_i/V_∞=3; θ=0°; (f) V_i/V_∞=3; θ=30°; (g) V_i/V_∞= 5; θ=0°; (h) V_i/V_∞=5; θ=30°
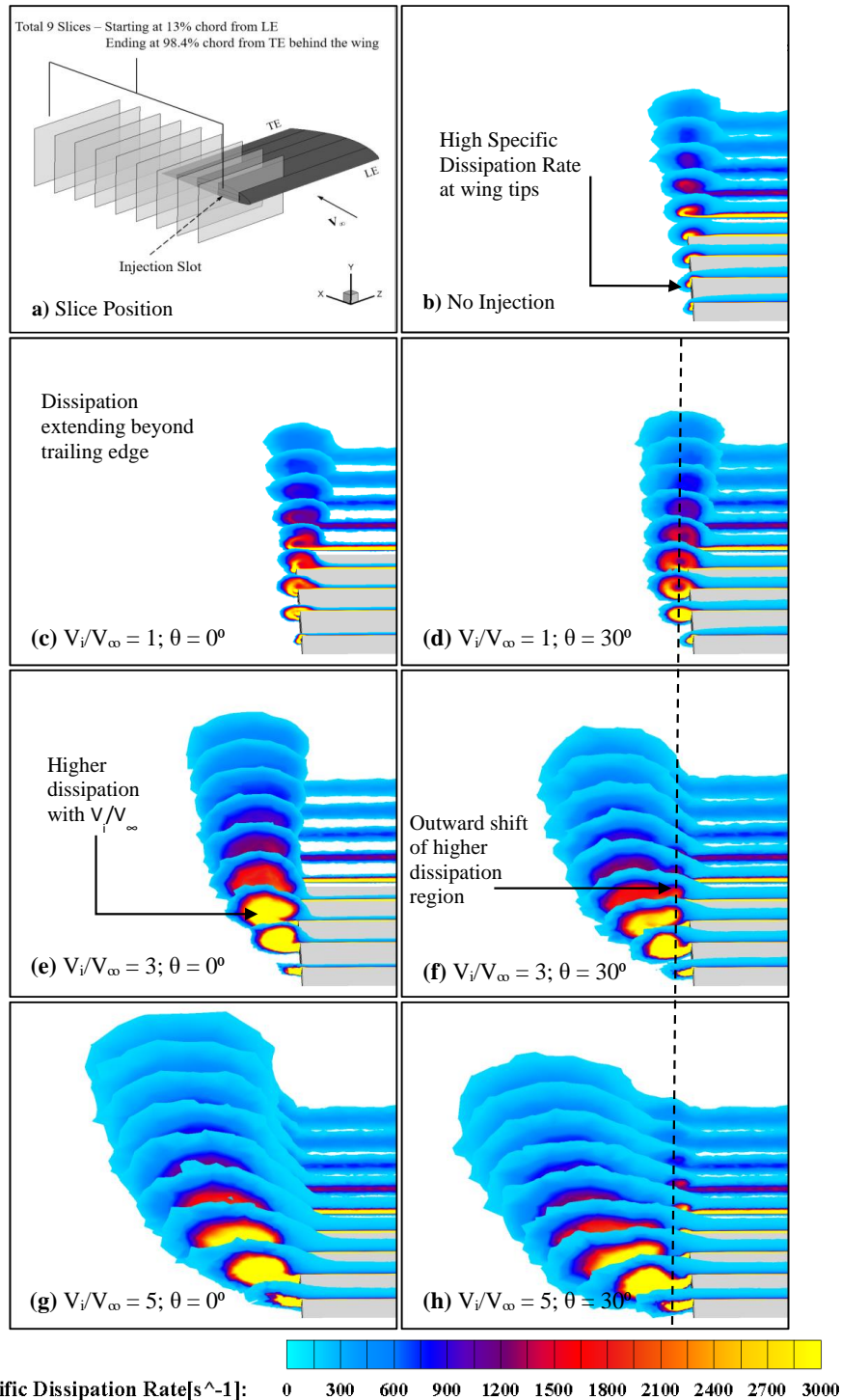
Fig. 9 Specific Dissipation (a) Slice Position; Contour plots for Specific Dissipation Rate (b) No Injection; (c) V_i/V_∞=1; θ=0°; (d) V_i/V_∞=1; θ=30°; (e) V_i/V_∞=3; θ=0°; (f) V_i/V_∞=3; θ=30°; (g) V_i/V_∞=5; θ=0°; (h) V_i/V_∞=5; θ=30°

as shown in Fig. 8(f). Further, when the injection velocity ratio is increased to 5, TKE is found to increase, as shown in Fig. 8(g). The stronger TKE region is shifted downward when the injection angle is 30°, and it is understood that the vortex is detached from the wing surface, as shown in Fig. 8(h). Overall, an additional vortex roll-up causes the production of TKE on a larger scale near the large-scale fluctuating motion. With the decrement of TKE over the wing, a higher lift is produced by introducing the winglet injection. By increasing the injection velocity, the high TKE region moves outward, increasing the lift. The inlet injection causes large TKE regions in the background, reducing large-scale turbulent fluctuation on the wing and thus keeping smooth flow over the wing.

Fig. 9 shows the distribution of specific dissipation rate (ω) with varying injection velocity ratios and angles. The slice positions and the dissipation rate at no injection case are shown in Fig. 9(a) and 9(b). A high dissipation rate is observed on the wing surface at no injection, especially near the wing tips. Further, the region of high specific dissipation gets shifted outwards of the wing tip with injection, as shown in Fig. 9(c), and the regions with a larger specific dissipation rate shifted downward for a higher injection angle, as shown in Fig. 9(d). Further, the winglet injection has a lower dissipation rate over the wing surface. The drag reduced for higher injection angle may be due to the outward shift of high dissipation rate regions (Roy *et al*. 2021). In Fig. 9(e), the specific dissipation rate for the injection velocity ratio 3 is shown, and the specific dissipation rate is low near the wing. Also, the injection angle shifted the higher dissipation region outward, as shown in Fig. 9(f). At injection velocity ratio 5, the dissipation rate over the wing reduces drastically, as shown in Fig. 9(g), resulting in lesser drag. The same phenomena for the 30° injection with some outward shift of the higher dissipation region, as shown in Fig. 9(h), results in drag reduction.

It is evident that by introducing winglet injection, a large area of TKE and specific dissipation rate moved away from the wing, reducing the turbulent fluctuations and dissipation rate. Thus we can conclude that the winglet injection works as an extended part of the wing, and wing tip vortices along with turbulence rollup shifted towards the extended wingtip, keeping the flow over the wing as it should be for the infinite wing, which eventually increases the lift and reduces the drag.

5. Conclusions

Various active flow control techniques to reduce wing tip vortices have been extensively studied in the past. Spanwise blowing from wingtips was one of the prime active flow control techniques that need more investigation to explore several factors' effects on its performance. In this study, the concept of using high-velocity wingtip jet injection at different injection angles was numerically investigated. The jet injection significantly improved lift, drag, and aerodynamic efficiency. In particular, the lift increases with an increase in jet velocity and decreases with an increase in jet injection angle. The drag coefficient behaves more complexly but decreases with high injection velocity and greater injection angle. By plotting streamline, different aerodynamics, and turbulent parameters, the behaviors of lift and drag coefficients. The apparent increase in wing aspect ratio due to injection makes the flow smoother over the wing by shifting the wingtip vortices and large-scale turbulence outward. From streamline plots, the vortex alterations are visible, and it was found that the injection velocity and angles dictate the extent of the vortex shift. The increase in lift is also investigated by the increase in pressure difference at the wingtip, as seen

in the pressure plots.

The study's primary aim was to propose a range of injection velocities and angles to implement in aircraft. The present study shows that the maximum aerodynamic efficiency for injection angle θ=30° with a high injection velocity of V_i/V_∞ greater than 3. Thus these conditions are the most optimal settings for using wing tip injection for vortex attenuation.

Future work of this study entails the physical model creation of the proposed fluidic winglet and conducting experimental wind tunnel tests. Further, this study has not covered the pulsed periodic jet injection regimes, which can be researched upon carrying out similar studies. With the maturity of fluidic winglets, they can be applied in aircraft in the real world. A successful application will improve endurance and range for aircraft equipped with this technology.

References

Ayers, R.F. and Wilde, M.R. (1956), "Aerodynamic characteristics of a swept wing with spanwise blowing".

Briggs, M. and Schwind, R. (1983), "Augmentation of fighter aircraft lift and STOL capability by blowingoutboard from the wing tips", *21st Aerospace Sciences Meeting*, 78.

Carafoli, Ej. and Camarasescu, N. (1971), "New researches on small span-chord ratio wings with lateral jets", Foreign Technology Division, Wright-Patterson AFB, Ohio.

Carafoli, E. (1962), "The influence of lateral jets, simple or combined with longitudinal jets, upon the wing lifting characteristics", *Proceedings of the 3rd ICAS Congress*, Stockholm.

Childs, R.E. (1986), "Lift augmentation via spanwise tip blowing: A numerical study", *24th Aerospace Sciences Meeting*, January.

Coimbra, R.F.F. and Catalano, F.M. (2002), "The effect of wing tip blowing on the vortex drag", *ICAS 2002*.

Crow, S.C. (1970), "Stability theory for a pair of trailing vortices", *AIAA J.*, **8**(12), 2172-2179.

Deslich, J. and Gunasekaran, S. (2019), "Effect of slotted winglet on the wingtip vortex", *AIAA Aviation 2019 Forum*, 3431.

Dghim, M., Ferchichi, M. and Benchiekh, M. (2014), "Control of wing tip vortex structure using fluidic actuation", *7th AIAA Flow Control Conference*, 2792.

Dghim, M., Ferchichi, M., Perez, R.E. and BenChiekh, M. (2016), "Near wake development of a wing tip vortex under the effect of synthetic jet actuation", *Aerosp. Sci. Technol.*, **54**, 88-107. https://doi.org/10.1016/j.ast.2016.04.008.

Duraisamy, K. and Baeder, J. (2003), "Control of tip-vortex structure using steady and oscillatory blowing", *21st AIAA Applied Aerodynamics Conference*, 3407.

Dutta, D., Dasgupta, A., Lawrence Raj, P.R. and Debnath, K. (2022), "Drag reduction and turbulent characteristics of a low aspect ratio wing with fluidic on-demand winglet", *SAE Int. J. Aerosp.*, **16**(1), 1-16. https://doi.org/10.4271/01-16-01-0003.

Gunasekaran, S. and Gerham, T. (2018), "Effect of chordwise slots on aerodynamic efficiency and wingtip vortex", *AIAA J.*, **56**(12), 4752-4767.

Gursul, I. and Wang, Z. (2018), "Flow control of tip/edge vortices", *AIAA J.*, **56**(5), 1731-1749.

Holloway, A.G.L. and Richardson, S. (2007), "Development of a trailing vortex formed with spanwise tip jets", *J. Aircraft*, **44**(3), 845-857.

Kroo, I. (2001), "Drag due to lift: Concepts for prediction and reduction", *Ann. Rev. Fluid Mech.*, **33**(1), 587-617.

Lappas, I. and Ikenaga, A. (2019), "Conceptual design and performance optimization of a tip device for a regional turboprop aircraft", *Aerosp.*, **6**(10), 1-22. https://doi.org/10.3390/aerospace6100107.

Lim, H.B. (1994), *Numerical Study of the Trailing Vortex of a Wing with Wingtip Blowing*, Stanford University.

Liu, D., Song, B., Yang, W., Yang, X., Xue, D. and Lang, X. (2021), "A brief review on aerodynamic

performance of wingtip slots and research prospect", *J.Bionic Eng.*, **18**, 1255-1279. https://doi.org/10.1007/s42235-021-00116-6.

Margaris, P. and Gursul, I. (2010), "Vortex topology of wing tip blowing", *Aerosp. Sci. Technol.*, **14**(3), 143-160. https://doi.org/10.1016/j.ast.2009.11.008.

Margaris, P. and Gursul, I. (2004), "Effect of steady blowing on wing tip flowfield", *2nd AIAA Flow Control Conference*, 2619.

Menter, F.R. (1993), "Zonal two equation κ-ω turbulence models for aerodynamic flows", *AIAA 23rd Fluid Dynamics, Plasmadynamics, and Lasers Conference*, July. https://doi.org/10.2514/6.1993-2906.

Menter, F.R. (1994), "Two-equation eddy-viscosity turbulence models for engineering applications", *AIAA J.*, **32**(8), 1598-1605. https://doi.org/10.2514/3.12149.

Mineck, R.E. (1995), "Study of potential aerodynamic benefits from spanwise blowing at wingtip", Nasa Technical Paper, June.

Narayan, G. and John, B. (2016), "Effect of winglets induced tip vortex structure on the performance of subsonic wings", *Aerosp. Sci. Technol.*, **58**, 328-340. https://doi.org/10.1016/j.ast.2016.08.031.

Okada, S. and Hiraoka, K. (2003), "Experimental studies of reduction of the wing tip vortex by suction", *21st AIAA Applied Aerodynamics Conference*. https://doi.org/10.2514/6.2003-3533.

Panagiotou, P., Kaparos, P. and Yakinthos, K. (2014), "Winglet design and optimization for a MALE UAV using CFD", *Aerosp. Sci. Technol.*, **39**, 190-205. https://doi.org/10.1016/j.ast.2014.09.006.

Roy, S., Barman, K., Debnath, K. and Mazumder, B.S. (2021), "Quantification of turbulent structures in and around the boundary region of a turbulent round jet released into counter-flow", *Measure.: J. Int. Measure. Confeder.*, **171**, 108758. https://doi.org/10.1016/j.measurement.2020.108758.

Selig, M.S., Guglielmo, J.J., Broeren, A.P. and Giguère, P. (1995), *Summary of Low Speed Airfoil Data*, SOARTECH Publications.

Simpson, R.G., Ahmed, N.A. and Archer, R.D. (2002), "Near field study of vortex attenuation using wing-tip blowing", *Aeronaut. J.*, **106**(1057), 117-120.

Skarolek, V. and Karabelas, S.J. (2016), "Energy efficient active control of the flow past an aircraft wing: RANS and LES evaluation", *Appl. Math. Model.*, **40**(2), 700-725. https://doi.org/10.1016/j.apm.2015.09.028.

Tavella, D.A., Wood, N.J. and Harrits, P. (1985), "Influence of tip blowing on rectangular wings", *3rd Applied Aerodynamics Conference*, October.

Tavella, D.A., Wood, N.J., Lee, C.S. and Roberts, L. (1986), "Two blowing concepts for roll and lateral control of aircraft", Technical Report, Joint Institute for Aeronautics and Acoustics, JIAA TR.

Tavella, D.A., Wood, N.J., Lee, C.S. and Roberts, L. (1988), "Lift modulation with lateral wing-tip blowing", *J. Aircraft*, **25**(4), 311-316. https://doi.org/10.2514/3.45565.

Van Doormaal, J.P. and Raithby, G.D. (1984), "Enhancements of the simple method for predicting incompressible fluid flows", *Numer. Heat Transf.*, **7**(2), 147-163. https://doi.org/10.1080/01495728408961817.

Vedamanickam, S., Ragni, D., de Oliveira, G. and Veldhuis, L. (2018), "Aerodynamics of an aircraft propeller model with passive tip jet", *J. Aircraft*, **55**(3), 1276-1286.

Whitcomb, R.T. (1976), "A design approach and selected wind tunnel results at high subsonic speeds for wing-tip mounted winglets", No. L-10908.

White, H.E. (1963), "Wind-tunnel investigation of the use of wing tip blowing to reduce drag for take-off and landing", David Taylor Model Basin, Washington DC.

Wood, N.J. and Roberts, L. (1988), "Control of vortical lift on delta wings by tangential leading-edge blowing", *J. Aircraft*, **25**(3), 236-243. https://doi.org/10.2514/3.45583.

Wu, J.M., Vakili, A. and Chen, L. (1983), *Wingtip Jets*.

Wu, J., Vakili, A., Chen, Z. and Gilliam, F. (1983), "Investigations on the effects of discrete wingtip jets", *21st Aerospace Sciences Meeting*, January.

EC